International Journal of Advanced Technology and Engineering Exploration, Vol 9(93)
ISSN (Print): 2394-5443 ISSN (Online): 2394-7454
http://dx.doi.org/10.19101/IJATEE.2021.874994

Research Article

Analysis of subthreshold swing in junctionless cylindrical surrounding gate MOSFET using Gaussian doping profile

Hakkee Jung*
Department of Electronic Engineering, Kunsan National University, Gunsan 54150, Korea

Received: 08-October-2021; Revised: 06-August-2022; Accepted: 12-August-2022
©2022 Hakkee Jung. This is an open access article distributed under the Creative Commons Attribution (CC BY) License, which permits unrestricted use, distribution, and reproduction in any medium, provided the original work is properly cited.

Abstract
The subthreshold swing (SS) model is presented for a junctionless cylindrical surrounding gate (JLCSG) metal oxide semiconductor field effect transistor (MOSFET) with a Gaussian doping profile. Since the Poisson's equation using the Gaussian doping profile has no closed form solution in cylindrical coordinate, the potential distribution is obtained using the Taylor series expansion of the error function and exponential function. The SS model presented in this study is considered to be reasonable, comparing the SSs of 3D simulation and other papers. As a result, the smaller the projected range R_p and straggle σ_p , the smaller the SS. However, when the projected range is 1/2 of the silicon radius R, the SS remains constant regardless of the change of the straggle. The SS increases when straggle increases in R_p<R/2, whereas the SS decreases when straggle increases in R_p>R/2. Therefore, the SS should be kept low by adjusting the projected range and straggle in JLCSG MOSFET with gaussian doping profile.

Keywords
Cylindrical surrounding gate, Junctionless, Gaussian, Projected range, Straggle, Subthreshold swing.

1.Introduction

Due to the intensification of the short channel effect (SCE) by the decrease in the size of the transistor, the research on the structure of the 3D transistor to reduce it has been very advanced [1−6]. The most commonly used FinFET has a tri-gate structure, and the channel is surrounded by three sides, and the flow of carriers in the channel can be controlled by using three gate terminals [7−12]. The more complete structure is the cylindrical structure [13−17]. The advantage is that the SCE can be very effectively reduced by surrounding the entire channel with a gate to control the flow of carriers in the channel. The cylindrical structure metal oxide semiconductor field effect transistor (MOSFET) can eliminate corner effects and realize high packing density due to the improved amount of current [18−19]. In particular, it is structurally operated in a volume conduction mode when a cylindrical MOSFET is fabricated in a junctionless structure. Thus, reducing surface roughness scattering that occurs in junction-based MOSFETs, enabling faster switching operation [20−24].

In addition, in the case of junctionless MOSFETs, the process is easy because the abrupt junction that occurs during the process can be avoided [25−30]. Based on these advantages, this study will analyze the subthreshold swing (SS) among SCEs for junctionless cylindrical surrounding gate (JLCSG) MOSFETs.

Even for a JLCSG MOSFET, SCEs such as an increase in tunneling current, a decrease in SS, a threshold voltage roll-off, and an increase in drain induced barrier lowering (DIBL) is inevitable physical phenomena when the transistor size decreases. In the case of a junctionless or junction-based cylindrical MOSFET, many researchers have analyzed the characteristics below the threshold voltage when the channel has a constant doping distribution [31−36]. In particular, Li et al.[37] divided channels or gates into 2-3 sections to observe changes such as SS and threshold voltage roll-off, and Lagraf et al. [38] divided the channels into 3 sections and compared the changes in threshold voltage and SS according to the ratio of each section using only constant doping distribution. However, in practice, the doping process is performed as a diffusion or ion implantation process, and it is very difficult to make the doping distribution constant

*Author for correspondence

within the channel due to the nature of the process. At this time, it is known that the doping distribution shows a Gaussian distribution. Therefore, using the doping distribution formed by the actual doping process, the potential distribution should be obtained and the SCEs should be analyzed. In order to obtain the potential in the channel using the Gaussian distribution function, the doping distribution function of the right hand in the Poisson equation must be described as the Gaussian function. It is difficult to obtain the analytical integral value of the Gaussian distribution function, so instead many researchers use the Gaussian-like doping profile [39−41].

This paper intends to present the analytical SS model of the JLCSG MOSFET with the doping distribution of the Gaussian function. Firstly, the Poisson equation is solved using the original Gaussian distribution function rather than the Gaussian-like doping profile to obtain the potential distribution for the JLCSG MOSFET. To this end, an approximating approach will be discussed since the Gaussian distribution function cannot be integrated directly. An analytical SS model will be presented using the potential distribution obtained in this way. The Gaussian distribution function has variables of the projected range and straggle, so the change of the SS will be analyzed for the change of these two variables. The results of this model will be compared with the case of uniform doing obtained by 3-D numerical device simulator DESSIS and other paper [42] to show the validity.

This paper is organized as follows: In sections 1 and 2, the necessity of Gaussian doping profile in the Poisson equation to accurately interpret the SS will be introduced, and the direction of this paper will be described while referring to related literatures. Section 3 will explain the overall flow of this paper and the structure of the JLCSG MOSFET. And the potential distribution will be derived in an analytical form when the Gaussian doping profile is used in the Poisson equation, and the analytical form of SS will be presented using this potential distribution model. In section 4, we will prove the validity of this analytical SS derived from section 3 by comparing it with the results of DESSSIS, and use this model to analyze the SS according to the change of the projected range and straggle, parameters of the Gaussian doping profile. Section 5 and 6 will discuss the results of section 4, and conclude by explaining the usefulness and limitations of this model.

2.Literature review

When ion implantation, an essential process in MOSFET fabrication, is used, the doping distribution is distributed like a Gaussian function. However, many studies have solved the Poisson equation by simply assuming a constant doping distribution due to the complexity of the calculation. Nevertheless, some studies have tried to solve the Poisson equation using the Gaussian doping profile. However, when solving a differential equation such as the Poisson equation, the integration of the Gaussian function becomes impossible. Therefore, a Gaussian-like doping profile is used.

Singh et al. [43] analyzed the threshold voltage using a Gaussian-like doping profile in junctionless double gate MOSFET. At this time, the change in the threshold voltage and DIBL for the projected range and straggle, which are variables of the Gaussian-like doping profile function, was analyzed. The advantage of using a Gaussian-like doping profile is that the solution can be analytically and easily obtained by solving the Poisson equation. Singh et al. using this model, suggested that the threshold voltage decreases as the straggle increases.

Sood et al. [44] solved the Poisson equation using the Gaussian distribution function in the case of the cylindrical MOSFETs, but only analyzed the potential distribution qualitatively. In particular, they used the approximation of the Taylor series expansion for Gaussian doping profile, but focused on the one-dimensional potential distribution in the radial direction by solving the Poisson equation in the radial direction of the cylindrical channel. However, not only the one dimensional solution to Poisson equation but also the two dimensional solution to the homogenous Laplace equation are to be obtained using the superposition method in this paper. In this way, the potential distribution in the channel length direction as well as in the radial direction can be obtained.

Mehta and Kaur [45] analyzed subthreshold behaviors for only double gate MOSFETs using Gaussian doping profile. However, in the case of a double-gate MOSFET, there are only two gate terminals that can control the carriers in the channel. As described above, the JLCGS MOSFET with the gate terminal covering the entire channel is a transistor that can reduce SCE than the double gate MOSFET, and TSMC and Samsung Electronics are doing their best to develop the JLCSG MOSFET

[46−47]. Therefore, future research on JLCSG MOSFETs will be very important.

Banerjee et al. [48] analyzed the SCEs such as threshold voltage, subthreshold swing and DIBL of a dual gate material JLCSG MOSFET using a Gaussian function. However, they also used the parabolic potential approximation to obtain the potential distribution in the channel direction. In particular, only junction-based MOSFETs with problems such as abrupt doping profile changes occurring at the channel and source/drain junctions in the miniaturization process were analyzed.

As can be seen from the above literature reviews, many researchers are trying to present a model for accurate SCEs analysis of JLCSG MOSFETs. It is clear that JLCSG MOSFET will play a very important role as a next-generation semiconductor device, so accurate analysis of it is essential. However, the analysis using the Gaussian doping profile, which is indispensable in the doping process, is insufficient. This is also due to the difficulty in integrating the Gaussian doping profile. To solve this problem, the goal of this paper is to solve the Poisson equation by approximating the function generated from the integration of the Gaussian doping profile with a Taylor series, and to obtain an analytical SS model using this potential distribution.

3.Methods

3.1Overview for presentation of the analytical SS model of JLCSG MOSFET with gaussian doping profile

The purpose of this paper is to present an analytical SS model for analyzing SS among SCEs of JLCSG MOSFETs with Gaussian doping profile as shown in *Figure 1*. For this, we must first find the analytical form of potential distribution. The potential distribution is composed of the sum of $\phi_1(r)$, which is a one-dimensional solution, and $\phi_2(r,z)$, which is a two-dimensional solution. At this time, the Poisson equation was solved analytically using the Gaussian doping profile. However, since the integral of the Gaussian function is analytically difficult when solving the Poisson equation, it was solved using an approximate equation by Taylor's series to derive $\phi_1(r)$. Using the analytical potential model obtained in this way, the analytical SS model was presented according to the definition of SS. At this time, r_{eff}, the conduction path and z_{min}, the z-value of the minimum potential were used. The validity of the presented analytical SS model will be verified by comparing it with the results of DESSIS and other paper. Using this model, changes in SS with respect to the projected range R_p and straggle σ_p will be considered. More details are provided in the next section.

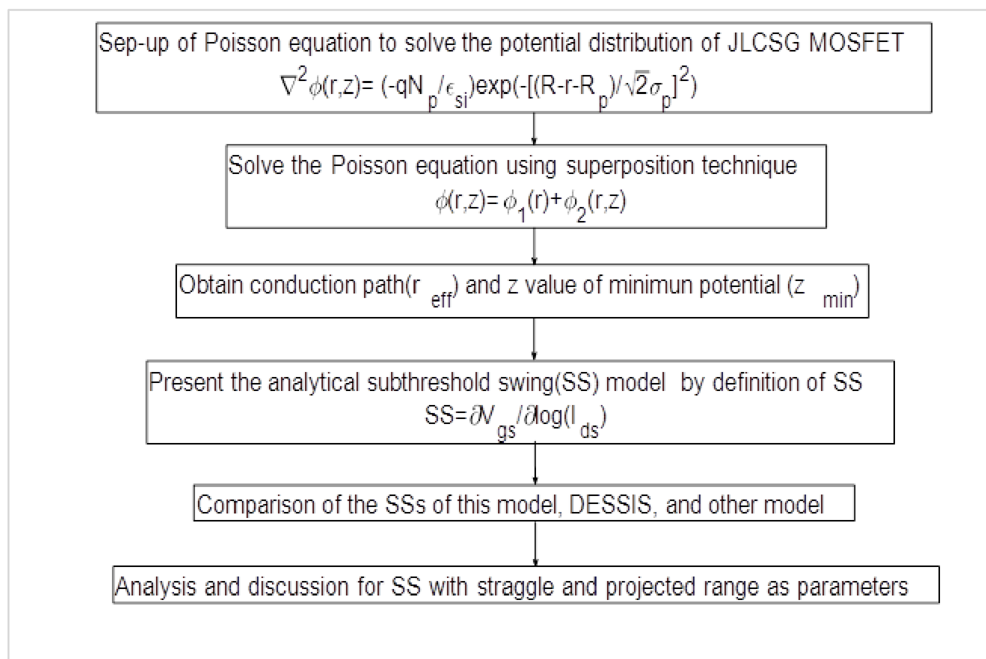

Figure 1 Block diagram of approach to present the analytical SS model for JLCSG MOSFET with Gaussian doping profile

3.2 Extraction of potential distribution using Gaussian distribution function

Figure 2 shows the schematic diagram of the JLCSG MOSFET. The source and drain is doped with n^+ type, and the channel is doped with a high concentration of n-type with Gaussian doping profile, and a metal with ϕ_m =4.7 eV is used as the gate metal. The L_g is the length of the channel, R is the radius of the silicon, and t_{ox} is the gate oxide thickness, and SiO_2 is used as gate oxide. The V_{gs}, V_{ds}, and V_s represent a gate voltage, a drain voltage, and a source voltage, respectively. At this time, the potential distribution of the JLCSG MOSFET is obtained using the following Poisson Equation 1.

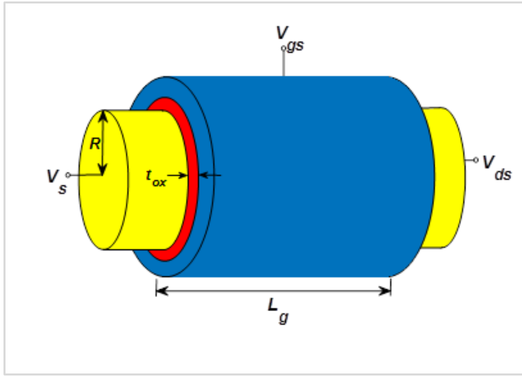

Figure 2 Schematic diagram of the JLCSG MOSFET

$$\frac{1}{r}\frac{\partial}{\partial r}\left[r\frac{\partial}{\partial r}\phi(r,z)\right]+\frac{\partial^2\phi(r,z)}{\partial z^2}=-\frac{qN_p}{\varepsilon_{si}}e^{-\left(\frac{(R-r)-R_p}{\sqrt{2}\sigma_p}\right)^2} \tag{1}$$

Here, ε_{si} is the dielectric constant of silicon, N_p is the peak doping concentration and 10^{18}/cm^3 is used, R_p is the projected range, and σ_p is the straggle to determine the shape of the Gaussian distribution function. Using the superposition technique, the electrostatic potential in channel region can be expressed as follows (Equation 2).

$$\phi(r,z)=\phi_1(r)+\phi_2(r,z) \tag{2}$$

Here $\phi_1(r)$ is the one dimensional solution to Poisson's equation and $\phi_2(r,z)$ is the two dimensional solution to the homogenous Laplace equation, which can be expressed as follows (Equation 3 and 4).

$$\frac{1}{r}\frac{\partial}{\partial r}\left(r\frac{\partial\phi_1(r)}{\partial r}\right)=-\frac{qN_p}{\varepsilon_{si}}e^{-\left(\frac{(R-r)-R_p}{\sqrt{2}\sigma_p}\right)^2} \tag{3}$$

$$\frac{\partial^2\phi_2(r,z)}{\partial r^2}+\frac{1}{r}\frac{\partial\phi_2(r,z)}{\partial r}+\frac{\partial^2\phi_2(r,z)}{\partial z}=0 \tag{4}$$

First, the following boundary condition is used to obtain $\phi_1(r)$ (Equation 5).

$$\left.\frac{\partial\phi_1(r)}{\partial r}\right|_{r=0}=0$$
$$\left.\frac{\partial\phi_1(r)}{\partial r}\right|_{r=R}=\frac{C_{ox}}{\varepsilon_{si}}\left[V_{gs}-\phi_{ms}-\phi_1(R)\right] \tag{5}$$

where ϕ_{ms} is the difference in work function between metal and semiconductor. The C_{ox} can be expressed as follows (Equation 6).

$$C_{ox}=\frac{\varepsilon_{ox}}{R\ln(1+t_{ox}/R)} \tag{6}$$

If Equation 3 is multiplied by r and integrated once,

$$r\frac{\partial\phi_1(r)}{\partial r}=\sqrt{\frac{\pi}{2}}\xi\sigma_p\left(R-R_p\right)erf\left(\frac{R-r-R_p}{\sqrt{2}\sigma}\right)+\xi\sigma_p^2\exp\left(-\left(\frac{R-r-R_p}{\sqrt{2}\sigma_p}\right)^2\right)+C$$

$$\xi=\frac{qN_p}{\varepsilon_{si}} \tag{7}$$

And the integral constant C is as follows using the boundary condition of Equation 5.

$$C=-\sqrt{\frac{\pi}{2}}\xi\sigma_p(R-R_p)erf\left(\frac{R-R_p}{\sqrt{2}\sigma_p}\right)-\xi\sigma_p^2\exp\left(-\left(\frac{R-R_p}{\sqrt{2}\sigma_p}\right)^2\right) \tag{8}$$

Dividing Equation 7 by r and then integrating once, the following equation can be obtained.

$$\phi_1(r)=\sqrt{\pi}\xi\sigma_p^2\left(R-R_p\right)\int\frac{erf(x)}{\sqrt{2}\sigma_p x-(R-R_p)}dx+\sqrt{2}\xi\sigma_p^3\int\frac{\exp\left(-x^2\right)}{\sqrt{2}\sigma_p x-(R-R_p)}dx+C\ln r+D$$

$$x=\frac{R-r-R_p}{\sqrt{2}\sigma_p} \tag{9}$$

where the D is constant. Since this integration cannot be expressed in an explicit form, it is approximated using the Taylor's series of *exp* and *erf* functions and then integrated. That is, if we rewrite Equation 9

using the approximation equation, it can be written as (Refer to *Appendix I* for function A_n)

$$\phi_1(r) = \sqrt{\pi}\xi\sigma_p^2\left(R-R_p\right)\frac{2}{\sqrt{\pi}}\int\frac{x-x^3/3+x^5/10-x^7/42}{\sqrt{2}\sigma_p x-(R-R_p)}dx$$
$$+\sqrt{2}\xi\sigma_p^3\int\frac{(1-x^2+x^4/2-x^6/6)}{\sqrt{2}\sigma_p x-(R-R_p)}dx+C\ln r+D$$
$$=2\xi\sigma_p^2\left(R-R_p\right)\left[A_1\left(\frac{R-r-R_p}{\sqrt{2}\sigma}\right)-\frac{1}{3}A_3+\frac{1}{10}A_5-\frac{1}{42}A_7\right]$$
$$+\sqrt{2}\xi\sigma_p^3\left[A_0-A_2+\frac{1}{2}A_4-\frac{1}{6}A_6\right]+C\ln r+D \tag{10}$$

Using Equations 5 and 10, the integral constant D can be calculated as follows.

$$D = V_{gs}-V_{fb}-\frac{\varepsilon_{si}}{C_f}\left\{\begin{array}{l}\sqrt{\frac{\pi}{2}}\xi\sigma_p\left(R-R_p\right)\dfrac{erf\left(\frac{-R_p}{\sqrt{2}\sigma_p}\right)}{R}\\ +\xi\sigma^2\dfrac{\exp\left(-\left(\frac{-R_p}{\sqrt{2}\sigma_p}\right)^2\right)}{R}+\dfrac{C}{R}\end{array}\right\}$$
$$-\left\{\begin{array}{l}2\xi\sigma_p^2\left(R-R_p\right)\left[A_1\left(\frac{-R_p}{\sqrt{2}\sigma_p}\right)-\frac{1}{3}A_3+\frac{1}{10}A_5-\frac{1}{42}A_7\right]\\ +\sqrt{2}\xi\sigma_p^3\left[A_0-A_2+\frac{1}{2}A_4-\frac{1}{6}A_6\right]+C\ln R\end{array}\right\} \tag{11}$$

Substituting Equations 8 and 11 into Equation 10, $\phi_1(r)$ can be obtained. Since the method of obtaining $\phi_2(r,z)$ using Equation 4 is independent of the doping distribution, it can be obtained by using the variable separation method and $\phi_2(r,z)$ can be derived from Gupta [49], method using the Fourier-Bessel series as follows.

$$\phi_2(r,z)=\sum_{n=1}^{\infty}\left[C_n\exp\left(\frac{\alpha_n z}{R}\right)+D_n\exp\left(-\frac{\alpha_n z}{R}\right)\right]\times J_0\left(\frac{\alpha_n r}{R}\right) \tag{12}$$

where α_n is eigenvalues that satisfy the following equation.

$$RJ_0(\alpha_n)-\frac{\varepsilon_{si}}{C_{ox}}\alpha_n J_1(\alpha_n)=0 \tag{13}$$

The C_n and D_n are obtained using the following boundary conditions in Equation 12.

$$\phi(r,z=0)=0$$
$$\phi(r,z=L)=V_{ds} \tag{14}$$

Here, V_{ds} is the drain voltage and the source is assumed to be grounded. At this time, because the first term dominates the whole series due to rapid decay of the Fourier-Bessel series, $\phi_2(r, z)$ is described with the C_1 and D_1 as follows.

$$\phi_2(r,z)=\left[C_1(r)\exp\left(\frac{\alpha_n z}{R}\right)+D_1(r)\exp\left(-\frac{\alpha_n z}{R}\right)\right]\times J_0\left(\frac{\alpha_n r}{R}\right) \tag{15}$$

$$C_1(r)=\frac{-\phi(r)\left[1-\exp\left(-\frac{\alpha_1 L}{R}\right)\right]+V_{ds}}{2\sinh\left(\frac{\alpha_1 L}{R}\right)J_0\left(\frac{\alpha_1 r}{R}\right)}$$

$$D_1(r)=\frac{-\phi(r)\left[\exp\left(\frac{\alpha_1 L}{R}\right)-1\right]-V_{ds}}{2\sinh\left(\frac{\alpha_1 L}{R}\right)J_0\left(\frac{\alpha_1 r}{R}\right)} \tag{16}$$

Substituting Equations 10 and 15 into Equation 2, we can obtain the potential distribution of the JLCSG MOSFET with Gaussian distribution in the channel. *Figure 3* shows the potential distribution obtained using Equations 2, 9, and 15. As can be seen in *Figure 3*, the potential distribution within the channel changes according to the projected range R_p and straggle σ_p, so the SS will also change according to the two variables.

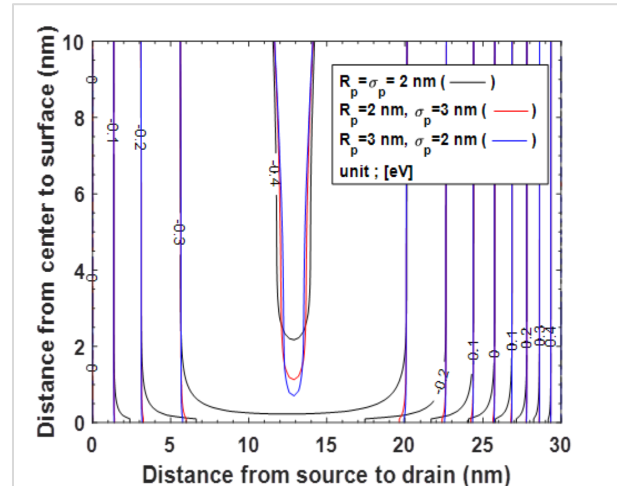

Figure 3 Potential distributions in the channel of JLCSG MOSFET with the projected range and straggle as parameters in the case of V_{ds}=0.5 V, V_{gs}=0.1 V and t_{ox}=2 nm

3.3 SS model extraction

The SS is defined as the change of the gate voltage when the drain current changes one order. Since the drain current is proportional to $e^{q\phi min/kT}$, it can be written as follows (Equation 17).

$$SS = \frac{\partial V_{gs}}{\partial \log(I_{ds})} = 2.3V_T \left[\frac{\partial \phi(r_{eff}, z_{\min})}{\partial V_{gs}} \right]^{-1} \quad (17)$$

Here, the r_{eff} is the conduction path, and it is known that most of the current flows to the center when the JLCSG MOSFET has a uniform doping distribution. However, the conduction path is a variable obtained by Equation 18 when the doping distribution in the channel has a Gaussian distribution function.

$$r_{eff} = \frac{\int r e^{-\left(\frac{R-r-R_p}{\sqrt{2}\sigma_p}\right)^2} e^{\phi(r,z_{\min})} dr}{\int e^{-\left(\frac{R-r-R_p}{\sqrt{2}\sigma_p}\right)^2} e^{\phi(r,z_{\min})} dr} \quad (18)$$

Here, the z_{min} is the z value where the minimum potential exists in the conduction path, so it can be calculated as follows if Equation 19 is solved.

$$\frac{\partial \phi(r_{eff}, z)}{\partial z} = \begin{bmatrix} C_1(r_{eff})\left(\frac{\alpha_1}{R}\right)\exp\left(\frac{\alpha_1 z}{R}\right) - \\ D_1(r_{eff})\left(\frac{\alpha_1}{R}\right)\exp\left(-\frac{\alpha_1 z}{R}\right) \end{bmatrix} = 0 \quad (19)$$

$$z_{\min} = \left(\frac{R}{2\alpha_1}\right) \ln\left(\frac{D_1(r_{eff})}{C_1(r_{eff})}\right) \quad (20)$$

In Equation 17, the derivative term can be found as follows.

$$\frac{\partial \phi(r_{eff}, z_{\min})}{\partial V_{gs}} = 1 + \left\{ \begin{array}{l} \frac{\partial C_1}{\partial V_{gs}} \exp\left(\frac{\alpha_1 z_{\min}}{R}\right) \\ + C_1 \frac{\partial}{\partial V_{gs}}\left[\exp\left(\frac{\alpha_1 z_{\min}}{R}\right)\right] \\ + \frac{\partial D_1}{\partial V_{gs}} \exp\left(-\frac{\alpha_1 z_{\min}}{R}\right) \\ + D_1 \frac{\partial}{\partial V_{gs}}\left[\exp\left(-\frac{\alpha_1 z_{\min}}{R}\right)\right] \end{array} \right\} \times J_0\left(\frac{\alpha_1 r_{eff}}{R}\right) \quad (21)$$

Substituting Equation 21 into Equation 17, the SS of the JLCSG MOSFET with Gaussian doping profile can be analytically obtained according to the projected range and straggle. The derivative value for V_{gs} on the right side of Equation (21) is shown in *Appendix II*. *Table 1* summarizes the device parameters used in this paper.

Table 1 Device parameters for this analytical SS model

Device parameter	Symbol	Value
Channel length	L_g	20-60 nm
Channel Radius	R	6-10 nm
SiO_2 thickness	t_{ox}	2 nm
Doping concentration	N_d	10^{18} /cm^3
Straggle	σ_p	2-10 nm
Projected range	R_p	2-6 nm

4.Results

First, in order to verify the validity of the model presented in this study, *Figure 4* shows the results of the Li's SS model [42] and DESSIS in the case of uniform doping. In the case of uniform doping in *Figure 4,* the doping concentration is 10^{18}/cm^3. As can be seen from *Figure 4*, the results of this SS model were in good agreement with the results of Li's model and DESSIS. When using the Gaussian doping profile, it can be observed that the SS changes according to the change of the straggle and the projected range that determines the shape of the distribution function.

In order to observe the change of the SS according to the change of the projected range and straggle in more detail, *Figure 5* shows a contour graph of the SS according to the change of the projected range and straggle in the case of channel lengths of 20 nm and 30 nm, a silicon radius of 10 nm, and a gate oxide thickness of 2 nm. As can be seen in *Figure 5*, the SS increases as the projected range increases. However, the change of SS with respect to the change of straggle is observed differently according to the range of the projected range. In other words, the SS increases as the straggle increases in the range where the projected range is less than 1/2 of the silicon radius that is R_p

<$R/2$, but the SS decreases as the straggle increases in the range of $R_p > R/2$. In addition, the change in SS appears more severe as the projected range increases, and the change in SS appears smaller as the straggle increases. In particular, the SS is shown regardless of straggle at $R_p=R/2$. In other words, we can find that the straggle is no longer an important variable for SS when the peak of the doping profile is in the middle of the silicon radius. As can be compared with *Figure 5(a)* and *(b),* it can be seen that the SS changes rapidly according to the projected range when the channel length decreases, and the change of SS with respect to the projected range becomes gentle when the channel length increases. If the straggle is more than 5 nm at L_g=30 nm, it can be observed that the change in SS is about 10% depending on the projected range. Therefore, as the channel length decreases, the SS changes greatly according to the projected range and straggle, so attention should be paid to the design of the JLCSG MOSFET. Note a sharp change in SS can be observed in the region of $R_p>R/2$ when the channel length is reduced.

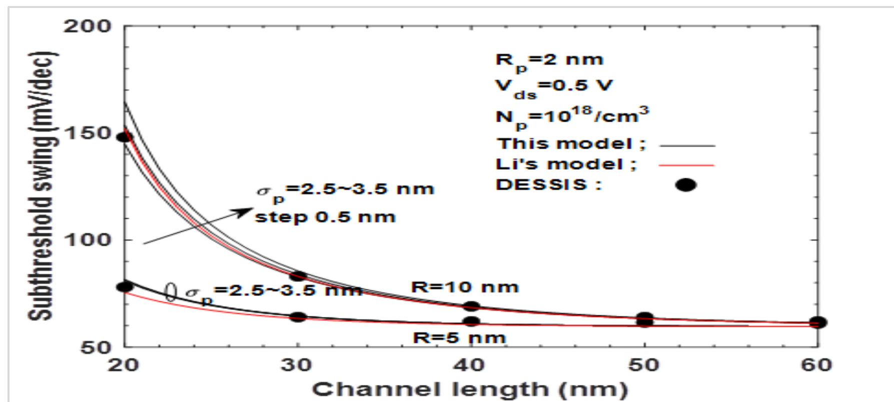

Figure 4 Comparison of SS versus channel length among this model (black lines), Li's model [42] (red lines), and DESSIS (dots) with the silicon radius as a parameter under the given conditions

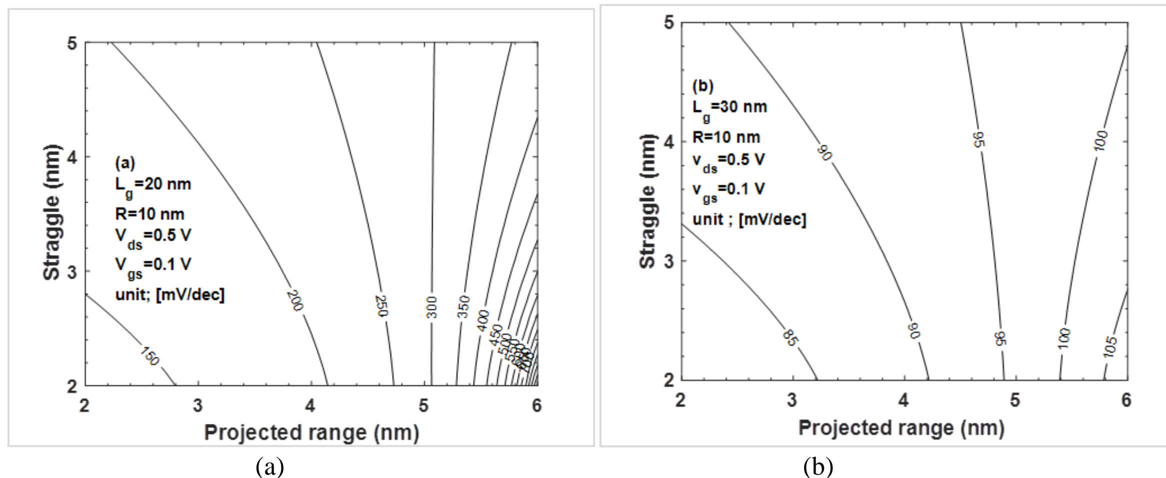

(a) (b)

Figure 5 Contours of SSs for projected range and straggle under the given conditions at (a) L_g=20 nm and (b) L_g=30 nm

In *Figure 4*, it can be observed that the smaller the channel length and the larger the silicon radius, the more the SS changes according to the straggle. The change of the SS according to the straggle is shown in *Figure 6* with the silicon radius and the projected range as parameters when the channel length is 20 nm. In *Figure 6 (a)* and *6 (b),* the SS increases as the silicon radius increases, and the SS significantly changes according to the change of the projected range. However, not only the SS decreases, but also the change of the SS according to the projected range decreases when the silicon radius decreases. The change of the SS according to the projected range is very small when R=6 nm, compared to the case of R=10 nm. As described above, since R =10 nm and R_p =5 nm in *Figure 6(a)* is the condition of $R_p=R/2$, so the

SS according to the change of straggle is observed almost constant. Similarly, since R=6 nm and R_p=3 nm in *Figure 6(b)* satisfies the condition of R_p=R/2, the SS according to the change of straggle is observed almost constant. In addition, it can be observed that the change trend of the SS with respect to the straggle changes with Rp=R/2 as the turning point. As the straggle increases, the change in the SS for the projected range change is very small. Also, the SS decreases as the projected range and straggle decrease, which can be observed in *Figure 6(a)* and *6(b).* In order to examine the change of the SS for the straggle in more detail, *Figure 7(a)* and *7(b)* are shown with the projected range and silicon radius as parameters.

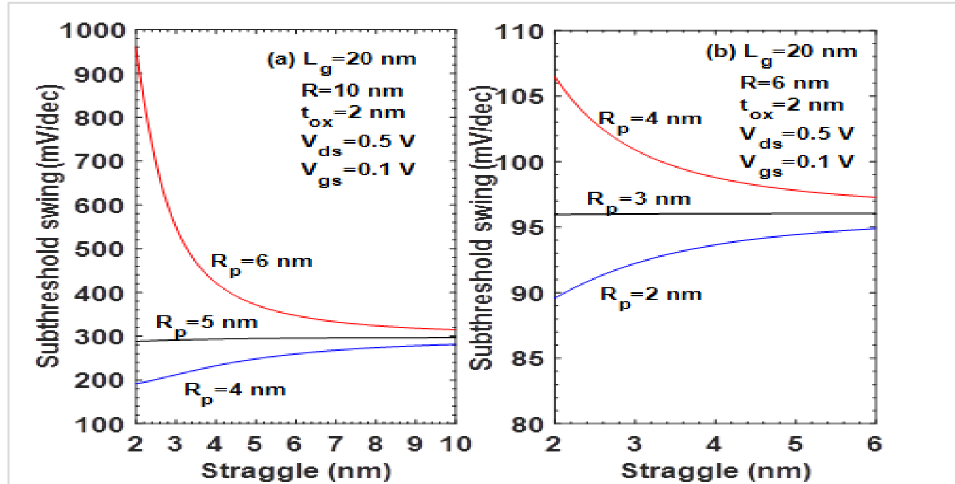

Figure 6 The SSs for the straggle with the silicon radius and projected range as parameters in the case of (a) R=10 nm and (b) R=6 nm under the given conditions

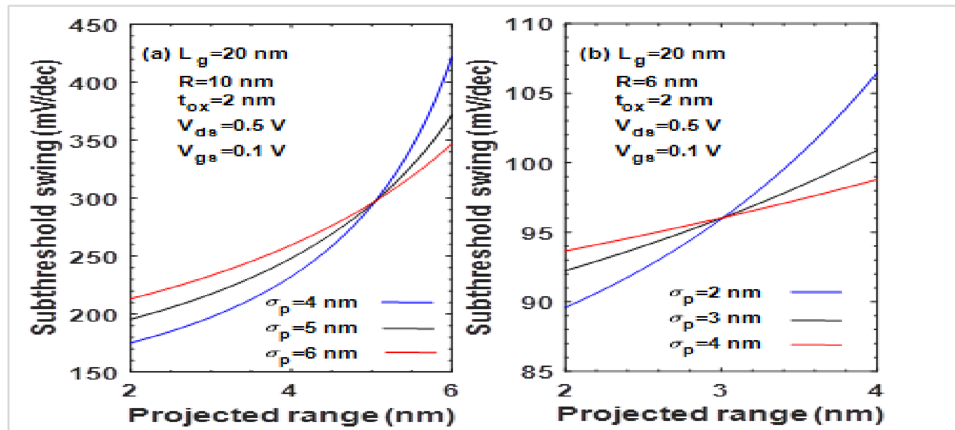

Figure 7 The SSs for the projected range with the silicon radius and straggle as parameters in the case of (a) R=10 and (b) R=6 nm under the given conditions

Comparing *Figure 6* and *Figure 7*, the SS increases as the projected range increases. However, in the case of R=10 nm in *Figure 7(a),* it can be observed that the magnitude of the SS changes according to the straggle with the turning point of R_p=R/2. This phenomenon is also observed in the case of R=6 nm in *Figure 7(b)*. In addition, as explained in *Figure 6(a)* and *6(b),* it can be observed *in Figure 7(a)* and *7(b)* that the SS shows a constant value at points of R_p=R/2 regardless of the straggle value.

The SS is ultimately a measure of how well the gate voltage can control the flow of carriers. Therefore, the closer the conduction path r_{eff} is to the gate terminal, the easier the control of conduction electrons by the gate voltage will be and the SS will decrease further. In order to examine this relationship, the change of conduction path for R=6 nm and 10 nm in the case of channel length of 20 nm is shown in *Figure 8* as a contour graph for the projected range and straggle. Comparing *Figure 5* and *Figure 8(a),* it can be

observed that the shape of the change is almost similar. That is, it can be seen that the conduction path is also fixed at almost 5 nm regardless of the straggle change at R_p=5 nm in the case of R=10 nm in *Figure 8(a)*. In addition, as the projected range increases and the conduction path gets closer to the central axis, the SS increases as it moves away from the gate terminal as shown in *Figure 5*. Note that, unlike in the case of uniform doping, the doping distribution changes according to the projected range and straggle in the case of Gaussian doping profile. This phenomenon can be observed even in the case of R=6 nm as shown in *Figure 8(b).* That is, in the case of R_p=3 nm, the conduction path is also constant at 3 nm regardless of the straggle. Therefore, as can be seen from *Figure 7(b)*, it shows a constant SS value at R_p=3 nm regardless of the straggle.

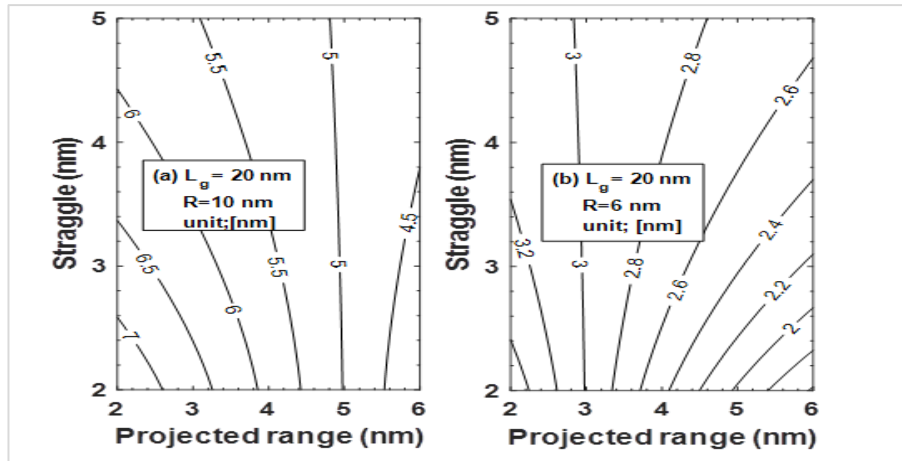

Figure 8 Contours of conduction paths for the projected range and straggle under the given conditions in the case of (a) L_g=20 nm, R=10 nm, and (b) L_g=20 nm, R=6 nm

5. Discussions

In this paper, an analytical SS model is presented to analyze the SS of JLCSG MOSFETs with Gaussian doping profile. Since it is difficult to obtain a uniform doping distribution in the actual doping process, the SCEs must be analyzed using the Gaussian doping profile. As the Gaussian function is affected by the projected range and the straggle, the resulting SS will also change according to these two variables. In this paper, the Poisson equation is solved using the Gaussian doping profile that changes according to the projected range and straggle, and the analytical potential distribution obtained at this time is used to derive the analytical SS model according to the definition of SS. As a result, within the useful range of the projected range and straggle of this model, the results of DESSIS and other papers were in good agreement with those of this model, so this model could be used to analyze the SS of JLCSG MOSFETs. As a result of the analysis, the SS was greatly affected by the projected range value if the straggle was small. That is, in the case of L_g = 20 nm and R = 6 nm, it can be seen that the SS increases from 89.5 mV/dec at the projected range of 2 nm to 106.5 mV/dec at the projected range of 4 nm if the straggle is a relatively small value of 2 nm. However, it can be seen that the SS only increases from 94 mV/dec at the projected range of 2nm to 99 mV/dec at the projected range of 4nm when the straggle increases to 4nm. In particular, it can be seen that the SS is constant regardless of the straggle value when the straggle value is 1/2 of the channel radius. The channel length has a great influence on the SS. It can be seen that not only SS increases when the channel length is decreased, but SS also changes significantly with changes in projected range and straggle. That is, if the straggle is 3 nm, the SS changes from about 150 mV/dec to 500 mV/dec when the channel length is 20 nm, the channel radius 10 nm, and the projected range changes from 2 nm to 6 nm. However, it can be seen that the SS changes from 84 mV/dec to 105 mV/dec under the same conditions when the channel length increases to 30 nm. In this paper, simulations were made for a channel length of 20-60 nm, a channel radius of 6-10 nm, and a gate oxide thickness of 2 nm. If the channel length is reduced to less than 10 nm, the quantum mechanical tunneling effect should be included.

A complete list of abbreviations is shown in *Appendix III.*

5.Conclusion

In this study, the change of SS among the SCEs of the JLCSG MOSFET with Gaussian doping profile was analyzed according to the projected range and straggle that determine the shape of the Gaussian doping profile. To this end, an analytical SS model using a potential distribution model was presented, and the validity of this model was verified by comparing the results of other papers and 2D simulation results. As a result of the analysis, it was observed that the SS increased and the rate of increase changed with straggle as the projected range increased. In other words, it can be seen that the SS decreases when the projected range and straggle decrease at the same time. In particular, when the projected range was placed at 1/2 of the silicon radius, it showed a constant SS regardless of the straggle. It was found that the factor that has the greatest influence on the SS value is the conduction path. The SS decreases as the conduction path approaches the gate contact, and it is found that the SS increases significantly due to the decrease in the control ability of the conduction electrons for the gate voltage, the further away from the gate contact. Therefore, in order to reduce the SS, the projected range and straggle value should be reduced to keep the conduction path as close to the gate contact as possible. This paper investigated only the case where the channel length is more than 20 nm, and if it becomes smaller than this, a model including quantum tunnelling phenomenon will be needed. In addition, if the doping profile is changed by the development of the doping process, a model corresponding to it should be presented.

Acknowledgment
None.

Conflicts of interest
The authors have no conflicts of interest to declare.

Author's contribution statement
Hakkee Jung: The author confirms sole responsibility for the following: study conception and design, data collection, analysis and interpretation of results, and manuscript preparation.

References

[1] Strempel K, Römer F, Yu F, Meneghini M, Bakin A, Wehmann HH, et al. Vertical 3D gallium nitride field-effect transistors based on fin structures with inverted p-doped channel. Semiconductor Science and Technology. 2020; 36(1):1-9.

[2] Owyeung RE, Sonkusale S, Panzer MJ. Opportunities for ionic liquid/ionogel gating of emerging transistor architectures. Journal of Vacuum Science & Technology B, Nanotechnology and Microelectronics: Materials, Processing, Measurement, and Phenomena. 2021; 39(1).

[3] Moon J, Nam S, Joo CW, Sung C, Kim HO, Cho SH, et al. Issues on monolithic 3D integration techniques for realizing next generation intelligent devices. Electronics and Telecommunications Trends. 2021; 36(3):12-22.

[4] https://www.copperpodip.com/post/gate-all-around-gaa-get-going-beyond-the-3-nanometer-mask. Accessed 18 July 2022.

[5] Subramanian S, Hosseini M, Chiarella T, Sarkar S, Schuddinck P, Chan BT, et al. First monolithic integration of 3d complementary fet (cfet) on 300mm wafers. In symposium on VLSI technology 2020 (pp. 1-2). IEEE.

[6] Gu Y, Wang C, Kim N, Zhang J, Wang TM, Stowe J, et al. Three-dimensional transistor arrays for intra-and inter-cellular recording. Nature Nanotechnology. 2022; 17(3):292-300.

[7] Shin J, Shin C. Experimental observation of zero DIBL in short-channel hysteresis-free ferroelectric-gated FinFET. Solid-State Electronics. 2019; 153:12-5.

[8] https://www.marketinsightsreports.com/reports/07158462998/global-finfet-cpu-matket-research-report-2022/inquiry?Mode=A28. Accessed 19 July 2022.

[9] Madhavi KB, Tripathi SL. Strategic review on different materials for FinFET structure performance optimization. In IOP conference series: materials science and engineering 2020 (pp.1-8). IOP Publishing.

[10] Park J, Kim J, Showdhury S, Shin C, Rhee H, Yeo MS, et al. Electrical characteristics of bulk FinFET according to spacer length. Electronics. 2020; 9(8):1-7.

[11] https:// eepower.com/technical-articles/what-is-a-finfet. Accessed 19 July 2022.

[12] https://english.cas.cn/newsroom/research_news/tech/202003/t20200310_230971.shtml. Accessed 19 July 2022.

[13] Zhang S. Review of modern field effect transistor technologies for scaling. In journal of physics: conference series 2020 (pp. 1-8). IOP Publishing.

[14] Yerragopu R, Priya DP, Kasthuribha JK. Modeling, optimization and comprehensive comparative analysis of 7nm FinFET and 7nm GAAFET devices. In AIP conference proceedings 2020 (pp.1-8). AIP Publishing LLC.

[15] Das UK, Bhattacharyya TK. Opportunities in device scaling for 3-nm node and beyond: FinFET versus GAA-FET versus UFET. IEEE Transactions on Electron Devices. 2020; 67(6):2633-8.

[16] Dash S, Mishra GP. An analytical model of the surface-potential-based source-pocket-doped cylindrical-gate tunnel FET with a work-function-modulated metal gate. Journal of Computational Electronics. 2020; 19(2):591-602.

[17] Shafizade D, Shalchian M, Jazaeri F. Charge-based modeling of ultra narrow junctionless cylindrical nanowire FETs. Solid-State Electronics. 2021.
[18] Abd EHH, Iñíguez B, Guitart JR. Analytical model of the threshold voltage and subthreshold swing of undoped cylindrical gate-all-around-based MOSFETs. IEEE Transactions on Electron Devices. 2007; 54(3):572-9.
[19] Ahn MJ, Saraya T, Kobayashi M, Hiramoto T. Variability characteristics and corner effects of gate-all-around (GAA) p-type poly-Si junctionless nanowire/nanosheet transistors. Japanese Journal of Applied Physics. 2021; 60(SB).
[20] Nowbahari A, Roy A, Marchetti L. Junctionless transistors: state-of-the-art. Electronics. 2020; 9(7):1-22.
[21] Ionescu AM. Nanowire transistors made easy. Nature Nanotechnology. 2010; 5(3):178-9.
[22] Bousari NB, Anvarifard MK, Haji-nasiri S. Improving the electrical characteristics of nanoscale triple-gate junctionless FinFET using gate oxide engineering. AEU-International Journal of Electronics and Communications. 2019; 108:226-34.
[23] Lü WF, Dai L. Impact of work-function variation on analog figures-of-merits for high-k/metal-gate junctionless FinFET and gate-all-around nanowire MOSFET. Microelectronics Journal. 2019; 84:54-8.
[24] Kumar A, Tiwari PK, Roy JN. Subthreshold model of asymmetric GAA junctionless FETs with scaled equivalent oxide thickness. Microelectronics Journal. 2022.
[25] Nowbahari A, Roy A, Nadeem AM, Marchetti L. Analysis of an approximated model for the depletion region width of planar junctionless transistors. Electronics. 2019; 8(12):1-19.
[26] Wang Y, Tang Y, Sun LL, Cao F. High performance of junctionless MOSFET with asymmetric gate. Superlattices and Microstructures. 2016; 97:8-14.
[27] Kumar B, Chaujar R. Analog and RF performance evaluation of junctionless accumulation mode (JAM) gate stack gate all around (GS-GAA) FinFET. Silicon. 2021; 13(3):919-27.
[28] Priyadarshani KN, Singh S, Mohammed MK. Gate-all-around junctionless FET based label-free dielectric/charge modulation detection of SARS-CoV-2 virus. RSC Advances. 2022; 12(15):9202-9.
[29] Jeon DY. Channel geometry-dependent threshold voltage and transconductance degradation in gate-all-around nanosheet junctionless transistors. AIP Advances. 2021; 11(5).
[30] Liu TY, Pan FM, Sheu JT. Characteristics of gate-all-around junctionless polysilicon nanowire transistors with twin 20-nm gates. IEEE Journal of the Electron Devices Society. 2015; 3(5):405-9.
[31] Jaafar H, Aouaj A, Bouziane A, Iñiguez B. An analytical drain current model for cylindrical gate DMG-GC-DOT MOSFET. International Journal of Electronics Letters. 2019; 7(4):458-72.
[32] Karbalaei M, Dideban D, Heidari H. A sectorial scheme of gate-all-around field effect transistor with improved electrical characteristics. Ain Shams Engineering Journal. 2021; 12(1):755-60.
[33] Maduagwu UA, Srivastava VM. Analytical performance of the threshold voltage and subthreshold swing of CSDG MOSFET. Journal of Low Power Electronics and Applications. 2019; 9(1):1-20.
[34] Kim JH, Sun WK, Park SH, Lim HI, Shin HS. A compact model of gate-voltage-dependent quantum effects in short-channel surrounding-gate metal-oxide-semiconductor field-effect transistors. JSTS: Journal of Semiconductor Technology and Science. 2011; 11(4):278-86.
[35] Thoti N, Li Y. Design of GAA nanosheet ferroelectric area tunneling FET and Its significance with DC/RF characteristics including linearity analyses. Nanoscale Research Letters. 2022; 17(1):1-11.
[36] Jung H. Analytical models of threshold voltage and drain induced barrier lowering in junctionless cylindrical surrounding gate (JLCSG) MOSFET using stacked high-k oxide. AIMS Electronics and Electrical Engineering. 2022; 6(2):108-23.
[37] Li C, Zhuang Y, Han R, Jin G. Subthreshold behavior models for short-channel junctionless tri-material cylindrical surrounding-gate MOSFET. Microelectronics Reliability. 2014; 54(6-7):1274-81.
[38] Lagraf F, Rechem D, Guergouri K, Zaabat M. Channel length effect on subthreshold characteristics of junctionless trial material cylindrical surrounding-gate MOSFETs with High-k gate dielectrics. Journal of Nano-and Electronic Physics. 2019; 11(2).
[39] Nandi A, Saxena AK, Dasgupta S. Analytical modeling of a double gate MOSFET considering source/drain lateral Gaussian doping profile. IEEE Transactions on Electron Devices. 2013; 60(11):3705-9.
[40] Shukla AK, Nandi A, Dasgupta S. Modeling source/drain lateral Gaussian doping profile of DG-MOSFET using green's function approach. Solid-State Electronics. 2020.
[41] Saha P, Banerjee P, Dash DK, Sarkar SK. Modeling short channel behavior of proposed work function engineered high-k gate stack DG MOSFET with vertical gaussian doping. In electron devices Kolkata conference 2018 (pp. 32-6). IEEE.
[42] Li C, Zhuang Y, Di S, Han R. Subthreshold behavior models for nanoscale short-channel junctionless cylindrical surrounding-gate MOSFETs. IEEE Transactions on Electron Devices. 2013; 60(11):3655-62.
[43] Singh B, Gola D, Singh K, Goel E, Kumar S, Jit S. Analytical modeling of channel potential and threshold voltage of double-gate junctionless FETs with a vertical Gaussian-like doping profile. IEEE Transactions on Electron Devices. 2016; 63(6):2299-305.
[44] Sood H, Srivastava VM, Singh G. Performance analysis of undoped and Gaussian doped cylindrical surrounding-gate MOSFET with it's small signal modeling. Microelectronics Journal. 2016; 57:66-75.

[45] Mehta H, Kaur H. Impact of Gaussian doping profile and negative capacitance effect on double-gate junctionless transistors (DGJLTs). IEEE Transactions on Electron Devices. 2018; 65(7):2699-706.
[46] http://www.businesskorea.co.kr/news/articleView.html?idxno=94884. Accessed 8 August 2022.
[47] https://www.phonearena.com/news/samsung-first-to-ship-3nm-gaa-chips_id141505. Accessed 8 August 2022.
[48] Banerjee P, Das J. Threshold voltage modeling of gaussian-doped dual work function material cylindrical gate-all-around (CGAA) MOSFET considering the effect of temperature and fixed interface trapped charges. Microelectronics Journal. 2022.
[49] Gupta SK. Threshold voltage model of junctionless cylindrical surrounding gate MOSFETs including fringing field effects. Superlattices and Microstructures. 2015; 88:188-97.

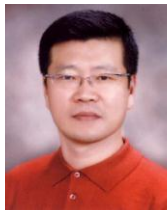

Prof. Hakkee Jung received the B.S. degree from Ajou University, Korea, in 1983, the M.S. and Ph.D. degrees from Yonsei University, Seoul, Korea, in 1985, 1990, respectively, all in Electronic Engineering. In 1990, he joined Kunsan National University, Chonbuk, Korea, where he is currently a Professor in the department of Electronic Engineering. From 1994 to 1995, he held a research position with the Electronic Engineering Department, Osaka University, Osaka, Japan. From 2004 to 2005, and 2016 to 2017, he was with the School of Microelectronic Engineering, Griffith University, Nathan, QLD, Australia. His research interests include Semiconductor Device Physics and Device Modeling.
Email: hkjung@kunsan.ac.kr

Appendix I Function A

In (10), the A_n function can be expressed as follows.

$$A_n = \int \frac{x^n}{\sqrt{2}\sigma_p x - (R - R_p)} dx$$

For $a = \sqrt{2}\sigma_p$, $b = -(R - R_p)$, it can be approximated by the following integral.

$$A_0(x) = \int \frac{1}{ax+b} dx = \frac{1}{a} \ln\left| x + \frac{b}{a} \right|$$

$$A_1(x) = \int \frac{x}{ax+b} dx = \frac{x}{a} - \frac{b}{a^2} \ln\left| x + \frac{b}{a} \right|$$

$$A_2(x) = \int \frac{x^2}{ax+b} dx = \frac{x^2}{2a} - \frac{bx}{a^2} + \frac{b^2}{a^3} \ln\left| x + \frac{b}{a} \right|$$

$$A_3(x) = \int \frac{x^3}{ax+b} dx = \frac{x^3}{3a} - \frac{bx^2}{2a^2} + \frac{b^2 x}{a^3} - \frac{b^3}{a^4} \ln\left| x + \frac{b}{a} \right|$$

$$A_4(x) = \int \frac{x^4}{ax+b} dx = \frac{x^4}{4a} - \frac{bx^3}{3a^2} + \frac{b^2 x^2}{2a^3} - \frac{b^3 x}{a^4} + \frac{b^4}{a^5} \ln\left| x + \frac{b}{a} \right|$$

$$A_5(x) = \int \frac{x^5}{ax+b} dx = \frac{x^5}{5a} - \frac{bx^4}{4a^2} + \frac{b^2 x^3}{3a^3} - \frac{b^3 x^2}{2a^4} + \frac{b^4 x}{a^5} - \frac{b^5}{a^6} \ln\left| x + \frac{b}{a} \right|$$

$$A_6(x) = \int \frac{x^6}{ax+b} dx = \frac{x^6}{6a} - \frac{bx^5}{5a^2} + \frac{b^2 x^4}{4a^3} - \frac{b^3 x^3}{3a^4} + \frac{b^4 x^2}{2a^5} - \frac{b^5 x}{a^6} + \frac{b^6}{a^7} \ln\left| x + \frac{b}{a} \right|$$

$$A_7(x) = \int \frac{x^7}{ax+b} dx = \frac{x^7}{7a} - \frac{bx^6}{6a^2} + \frac{b^2 x^5}{5a^3} - \frac{b^3 x^4}{4a^4} + \frac{b^4 x^3}{3a^5} - \frac{b^5 x^2}{2a^6} + \frac{b^6 x}{a^7} - \frac{b^7}{a^8} \ln\left| x + \frac{b}{a} \right|$$

Appendix II Differential term for V_{gs} in (21)

$$\frac{\partial C_1}{\partial V_{gs}} = \frac{-\left[1 - \exp\left(-\frac{\alpha_1 L}{R}\right)\right]}{2\sinh\left(\frac{\alpha_1 L}{R}\right) J_0\left(\frac{\alpha_1 r_{eff}}{R}\right)}$$

$$\frac{\partial D_1}{\partial V_{gs}} = \frac{-\left[\exp\left(\frac{\alpha_1 L}{R}\right) - 1\right]}{2\sinh\left(\frac{\alpha_1 L}{R}\right) J_0\left(\frac{\alpha_1 r_{eff}}{R}\right)}$$

$$\frac{\partial}{\partial V_{gs}}\left[\exp\left(-\frac{\alpha_1 z_{\min}}{R}\right)\right] = -\frac{\alpha_1}{R}\exp\left(-\frac{\alpha_1 z_{\min}}{R}\right)\frac{\partial z_{\min}}{\partial V_{gs}}$$

$$\frac{\partial}{\partial V_{gs}}\left[\exp\left(\frac{\alpha_1 z_{\min}}{R}\right)\right] = \frac{\alpha_1}{R}\exp\left(\frac{\alpha_1 z_{\min}}{R}\right)\frac{\partial z_{\min}}{\partial V_{gs}}$$

$$\frac{\partial z_{\min}}{\partial V_{gs}} = \left(\frac{R}{2\alpha_1}\right)\frac{\partial}{\partial V_{gs}}\left(\ln D_1(r_{eff}) - \ln C_1(r_{eff})\right)$$

$$= \left(\frac{R}{4\alpha_1 \sinh\left(\frac{\alpha_1 L}{R}\right) J_0\left(\frac{\alpha_1 r_{eff}}{R}\right)}\right) \times \left[\frac{\left[1 - \exp\left(-\frac{\alpha_1 L}{R}\right)\right]}{C_1(r_{eff})} - \frac{\left[\exp\left(\frac{\alpha_1 L}{R}\right) - 1\right]}{D_1(r_{eff})}\right]$$

Appendix III

S. No.	Abbreviation	Description
1	3D	Three Dimension
2	DESSIS	Device Simulation for Smart Integrated Systems
3	DIBL	Drain Induced Barrier Lowering
4	JLCSG	Junction Less Cylindrical Surrounding Gate
5	MOSFET	Metal-Oxide-Semiconductor Field Effect Transistor
6	SCE	Short Channel Effect
7	SS	Subthre shold Swing